Originally published as:

Thickness of the lithosphere east of the Dead Sea Transform

Ayman Mohsen,[1,2] Rainer Kind,[1,3] Stephan V. Sobolev,[1,4] Michael Weber[1,5] and the DESERT Group

[1] *GeoForschungsZentrum, 14473 Potsdam, Germany. E-mail: ayman@gfz-potsdam.de*
[2] *Al-Najah National University, Nablus, Palestine*
[3] *Freie Universität, Berlin, Germany*
[4] *Institute of Physics of the Earth, Moscow, Russia*
[5] *Universität Potsdam, Germany*

SUMMARY
We use the *S* receiver function method to study the lithosphere at the Dead Sea Transform (DST). A temporary network of 22 seismic broad-band stations was operated on both sides of the DST from 2000 to 2001 as part of the DESERT project. We also used data from six additional permanent broad-band seismic stations at the DST and in the surrounding area, that is, in Turkey, Saudi Arabia, Egypt and Cyprus. Clear *S*-to-*P* converted phases from the crust–mantle boundary (Moho) and a deeper discontinuity, which we interpret as lithosphere–asthenosphere boundary (LAB) have been observed. The Moho depth (30–38 km) obtained from *S* receiver functions agrees well with the results from *P* receiver functions and other geophysical data. We observe thinning of the lithosphere on the eastern side of the DST from 80 km in the north of the Dead Sea to about 65 km at the Gulf of Aqaba. On the western side of the DST, the few data indicate a thin LAB of about 65 km. For comparison, we found a 90-km-thick lithosphere in eastern Turkey and a 160-km-thick lithosphere under the Arabian shield, respectively. These observations support previous suggestions, based on xenolith data, heat flow observations, regional uplift history and geodynamic modelling, that the lithosphere around DST has been significantly thinned in the Late Cenozoic, likely following rifting and spreading of the Red Sea.

Key words: Dead Sea Transform, *S* receiver functions, thickness of the lithosphere.

GJI Seismology

INTRODUCTION

The Dead Sea Transform (DST) is a major left lateral strike slip fault (e.g. Garfunkel *et al.* 1981) that accommodates the relative motion between the African and Arabian plates, connecting a region of extension in the Red Sea to the Taurus collision zone in the north (Fig. 1). From geological observations it is estimated that about 105 km of horizontal movement has occurred since it began to form in the Cenozoic about 20 Ma ago (Quennell 1958; Girdler 1990). The DST is a first-order structure in the Middle East. It is the main source of earthquakes in this region. Large earthquakes are known to have occurred along this fault over the historical period (Abou Karaki 1987; Ambraseys *et al.* 1994). The dynamics of the entire region is dominated by the slip of the Arabian and Sinai plates, with a slip rate of ∼5 mm yr^{-1} (Garfunkel *et al.* 1981; Klinger *et al.* 2000). The thickness of the lithosphere is one of the most important parameters to address the problems of plate tectonic processes, but the transition from the lithosphere to the asthenosphere is still poorly sampled by most seismic data, including the area of the DST. Various geophysical studies had been carried out in different parts of

the DST, such as refraction/reflection profiles (Makris *et al.* 1983; El-Isa *et al.* 1987a,b; Ginzburg & Ben-Avraham 1987; DESERT Group 2004; Mechie *et al.* 2005), local-source (Koulakov & Sobolev 2006) and teleseimic (Koulakov *et al.* 2006) tomographic studies as well as gravity studies (Al-Zoubi & Ben-Avraham 2002; Götze *et al.* 2006). Receiver functions (Mohsen *et al.* 2005; Hofstetter & Bock 2004) have provided information about the crustal structures in the DST area. Most of these studies suggest that the crustal thickness is about 30 to 38 km from west to east. A lower crustal discontinuity (LCD) is found on the eastern part of the DST, reaching a depth of 30 km (DESERT Group 2004; Mohsen *et al.* 2005; Mechie *et al.* 2005; Götze *et al.* 2006).

Ginzburg *et al.* (1979b, 1981) have reported a mantle reflected *P* phase of 8.6 km s^{-1} at a depth of 55 km along a profile from the southernmost part of the Gulf of Aqaba to the Dead Sea Basin. El-Isa (1990), using data of the station UNJ (located at about 32°N and 36°E) has noted such an upper mantle discontinuity at 55 km depth with a thickness of about 2 to 3 km and an apparent velocity of 8.4 km s^{-1}, and a deeper one at about 105 km depth with apparent velocity of 8.9 km s^{-1}. In between these refractors he inferred the
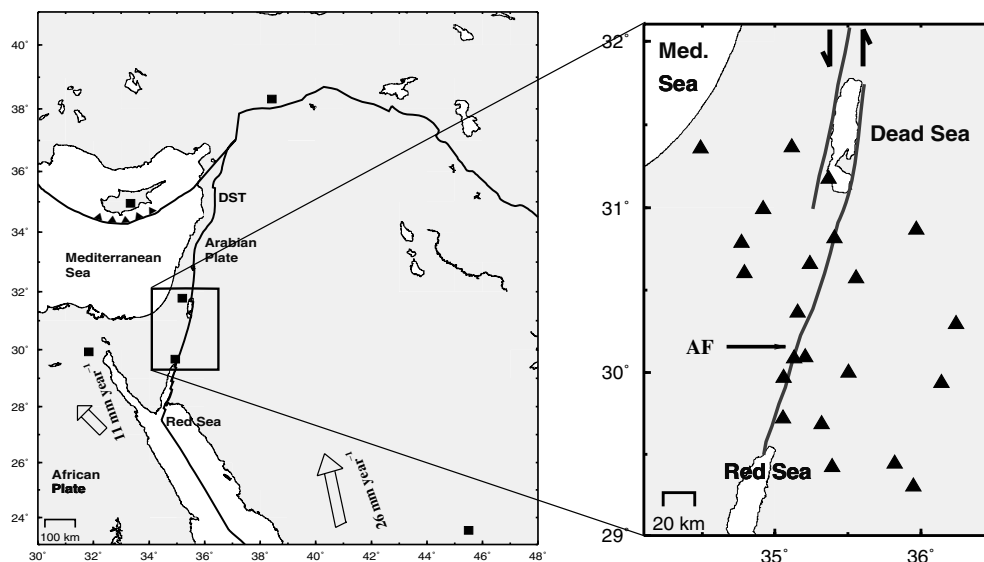
Figure 1. Tectonic setting of the Dead Sea Transform (DST). AF is the Araba Fault. The arrows indicate plate motion in millimetre per year, calculated relative to the fixed hotspots frame (Gripp & Gorden 1990). Closed triangles and closed squares represent the DESERT temporary seismic stations and the permanent stations, respectively.

presence of a low-velocity zone reaching its maximum at a depth of 80 km. From the shear wave velocity structure of the Sinai subplate and from a receiver function analysis, Hofstetter & Bock (2004) have reported a velocity decrease beginning at about 60–70 km beneath EIL and JER seismic stations (see Fig. 1 for the location). From a receiver function study across the DST, using about 50 broad-band and short period seismic stations, Mohsen (2004) has noticed a negative phase that arrives directly after the Moho at about 7 s delay time with respect to *P* along the DST. Julia *et al.* (2003) have reported from a joint inversion of receiver functions and surface wave group velocities, upper mantle shear velocities ranging from 4.3 to 4.6 km s^{-1} in the Arabian shield. They obtained temperatures around 1000°C from their velocity models for a thin upper mantle lid observed at one station in Saudi Arabia (TAIF) located at (21.40° latitude, 40.30° longitude), and suggest that the lithosphere could be as thin as 50 to 60 km under that station.

Mantle xenoliths from western Saudi Arabia, some 220 km east of the Red Sea margin, suggest that the lithosphere has been thinned by several tens of kilometres to its present calculated thickness of about 80 km or less (McGuire & Bohannon 1989; Stein *et al.* 1993). Geobarometric and geothermometric data from xenoliths suggest that the lithosphere under the Arabian rift shoulder is less than 80 km thick whereas the crust has a normal thickness of about 40 km (McGuire & Bohannon 1989). This would imply that the subcontinental lithospheric mantle underneath the Arabian rift shoulder was thinned without concomitant crustal thinning (Altherr *et al.* 1990), where volcanics directly related to the formation of the Red Sea commenced in Oligocene times and continued to historic times (Camp & Roobol 1989). Pressure–temperature estimates of xenoliths from Harrat Uwayrid (Saudi Arabia) led Henjes-Kunst (1989) to suggest that the LAB in that region is at a shallow depth of about 60 km. His estimates imply a significant amount of thermal erosion of the lower asthenosphere.

DATA

Fig. 1 shows the broad-band seismic stations used in this study. 22 seismic stations have been used from the DESERT temporary

seismic network, that had been set up in the area beginning of 2000 April for 1 yr (Mohsen *et al.* 2005). Six permanent seismic stations have been used from the surrounding area and are represented by closed squares in Fig. 1. Station KEG is located within the African plate about 50 km west of the northern end of the Gulf of Suez, delineating the western boundary of the Sinai plate. Station EIL is located on the margins of the Dead Sea rift, station JER is located about 30 km west of the Dead Sea rift, CSS is located in the centre of Cyprus, and RAYN is located on the Arabian shield. Station MALT is located in Malatya, Turkey, situated at the foot of the anti-Taurus Mountains. The waveform data of the DESERT temporary network and stations CSS, JER, EIL and MALT have been obtained from the GEOFON program of GeoForschungsZentrum (GFZ) Potsdam, Germany (Hanka *et al.* 2000), while waveform data of the KEG and RAYN have been obtained from the IRIS Data Management Center (Buttler *et al.* 2004). The coordinates of the stations used are listed in Table 1. *S* waves with high signal/noise ratio have been selected from earthquakes with magnitude larger than 5.6 and at epicentral distances of 60° to 85°. Good *S*-to-*P* conversion from the *S* phase can be observed in this distance range (Yuan *et al.* 2006). The distribution of the selected events is shown in Fig. 2. We note that almost all events are in the E–NE quadrant, only few events are in the south, and no event in the NW quadrant.

The recently developed *S* receiver function technique can be used to identify the LAB (Farra & Vinnik 2000; Li *et al.* 2004; Kumar *et al.* 2005, 2006a,b; Yuan *et al.* 2006). Low-velocity zones in the upper mantle usually derived with surface waves are frequently interpreted as asthenosphere. Therefore *S* receiver function observations of a negative discontinuity are frequently explained as observations of the LAB. We follow this interpretation. The *S* receiver function method searches for the *S*-to-*P* conversions at the seismic discontinuities beneath seismic stations. The converted phases arrive at the seismic station earlier than the direct *S* waves (precursors).

In this method, the multiple reverberations appear later than the *S* arrival. This means that *S* receiver function conveniently separates the primary *S*-to-*P* conversions from the later multiples of the *S* arrival. Here we apply this method to look at the base of the lithosphere in the region of the DST and its surrounding area.

Table 1. Stations codes (ID), coordinates of stations used.

| ID	Latitude	Longitude
ID27	30.79	34.77
ID08	30.60	34.79
ID12	30.99	34.92
JS02	30.29	36.24
JD02	30.81	35.41
JS04	29.30	35.95
ID27	30.66	35.24
ID28	30.36	35.16
ID31	30.08	35.13
ID32	29.97	35.06
JD06	30.09	35.21
JS03	29.94	36.14
JS07	29.42	35.39
JW01	30.87	35.97
JW09	29.68	35.32
ID30	31.17	35.37
JD08	29.72	35.05
JK02	30.57	35.56
JS05	29.44	35.82
JW07	29.99	35.50
ID29	31.36	35.12
ID10	31.36	34.49
JER	31.77	35.19
EIL	29.67	34.95
CSS	34.96	33.33
MALT	38.31	38.43
KEG	29.93	31.83
RAYN	23.52	45.50
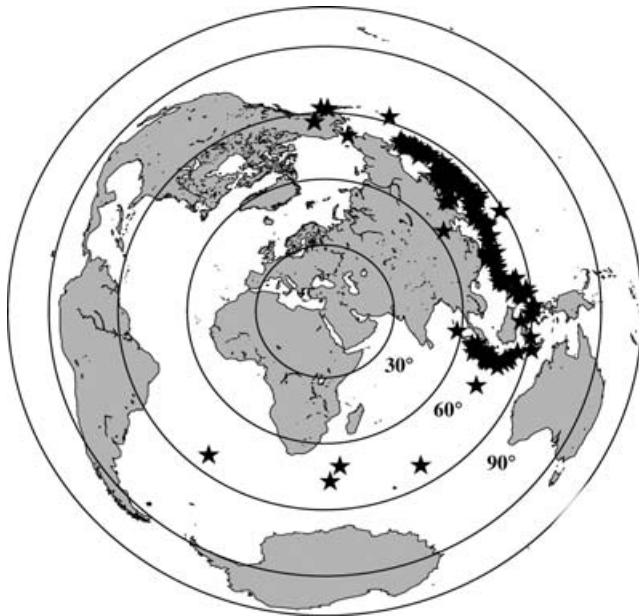
Figure 2. Distribution of teleseismic events with magnitude greater than 5.6 used in this study for *S* receiver functions. The circles indicate distance to the DESERT network in the Middle East in degrees.

To detect the *S*-to-*P* converted phases, the three component seismograms have to be rotated into the *P–SV–SH* (LQT) coordinate system (Li *et al.* 2004). After rotation, the converted *Sp* phases are primarily on the *L* component. The *P* components are deconvolved with the *S* signals on the SV components to equalize effects of different *S* signal forms. Therefore, the resulting *P* components, which contain only the converted *Sp* phases are called the *S* receiver
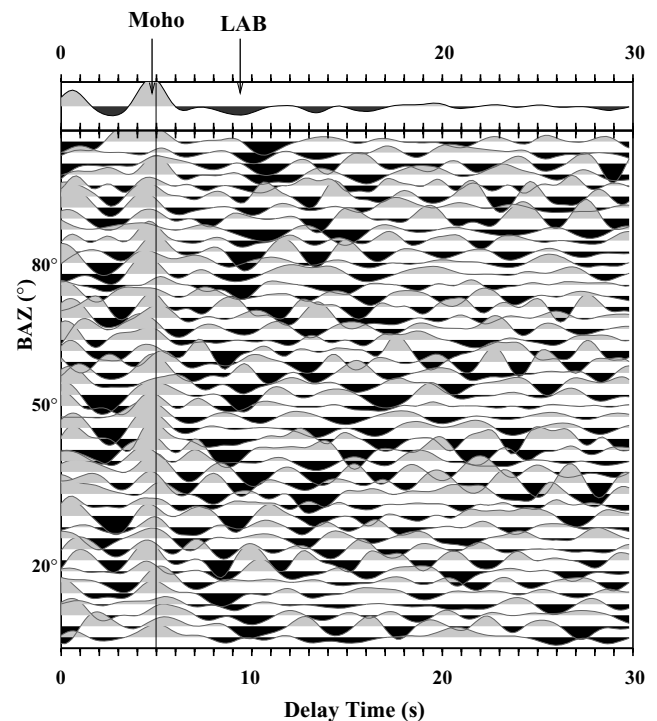
Figure 3. *S* receiver function for the permanent seismic station (MALT) in Turkey. The traces are plotted in a time window between 0 to 30 s and sorted by backazimuth (BAZ), indicated to the left of the traces. *S* arrival time is at zero seconds, and the time scale is reversed for better comparison with *P* receiver functions, that is, the abscissa represents the conversion time for *Sp* with respect to the *S* arrival time. The sum trace is displayed at the top. Two phases are visible, the positive Moho and the negative lithosphere-asthenosphere boundary (LAB).

functions. In this study, the incidence angle was determined by minimizing the *S* wave energy on the *P* component. A bandpass filter of 3–20 s has been applied. Similar to the *P* receiver function method, the sign of the receiver function signal is related to the contrast of the velocity. Positive converted phases from the Moho indicate velocity increase with depth, while the negative phases indicate velocity decrease. To make the *S*-to-*P* receiver functions directly comparable with the *P* receiver functions, the polarity of the *S* receiver functions and also the time axis have been reversed. In order to improve the signal-to-noise ratio, we summed *S* receiver functions of many earthquakes. We defined non-overlapping boxes near the DST, where all traces with piercing points at 80 km depth within one box are summed. As in the *P* receiver functions, we applied a moveout correction for *S*-to-*P* converted phases relative to a reference slowness of 6.4 s deg^{-1} before the summation step.

RESULTS

The *S* receiver functions of the permanent stations MALT in Turkey and RAYN in Saudi Arabia are plotted in Figs 3 and 4 in the time window between 0 to 30 s, respectively. The abscissa represents the conversion time of the *Sp* phases with respect to *S* arrival time, commonly denoted delay time.

The sum trace is displayed at the top. Two phases can be identified. The first is the positive *Sp* conversion from the Moho at about 5 s delay time in both permanent stations and the second one is a negative phase from the LAB at about 9.0 s at MALT and 16 s at RAYN. At both stations the Moho is a stronger phase than the LAB.
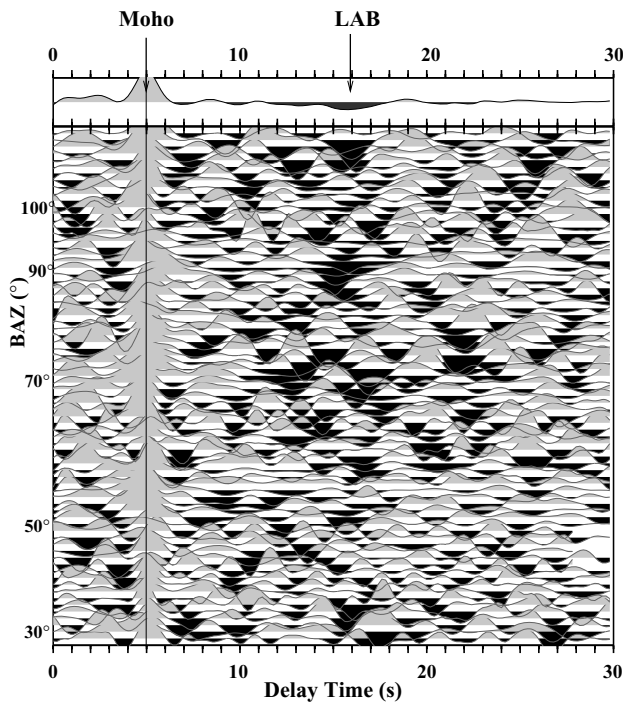
Figure 4. As Fig. 3 but for the permanent seismic station (RAYN) in Saudi Arabia.
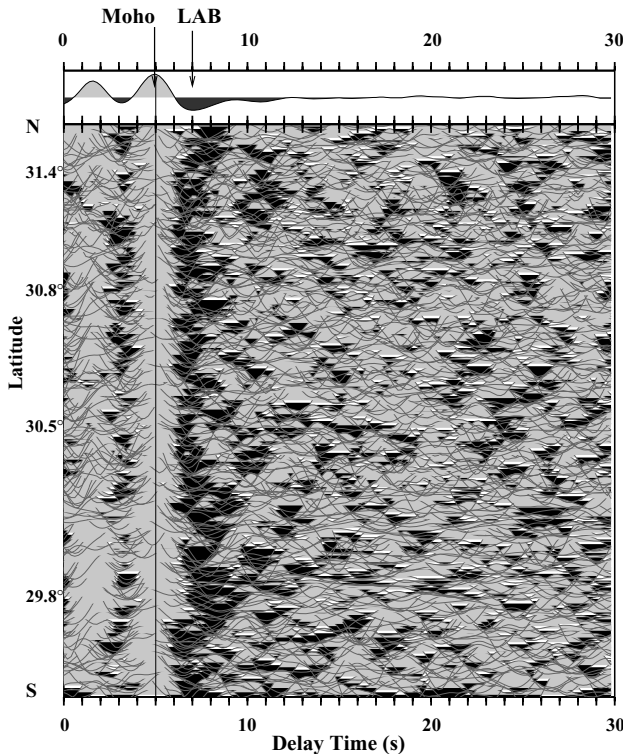

Figure 5. Plot of all *S* receiver functions obtained from the DESERT experiment. The traces are ordered according to the latitude of their piercing points (from south to north). Moho and the LAB are marked.

Fig. 5 shows the *Sp* receiver functions for all DESERT stations. As in Figs 3 and 4, the two prominent phases are the positive signal at about 5 s and a negative one at about 7 s, which are interpreted as the Moho and the LAB, respectively.
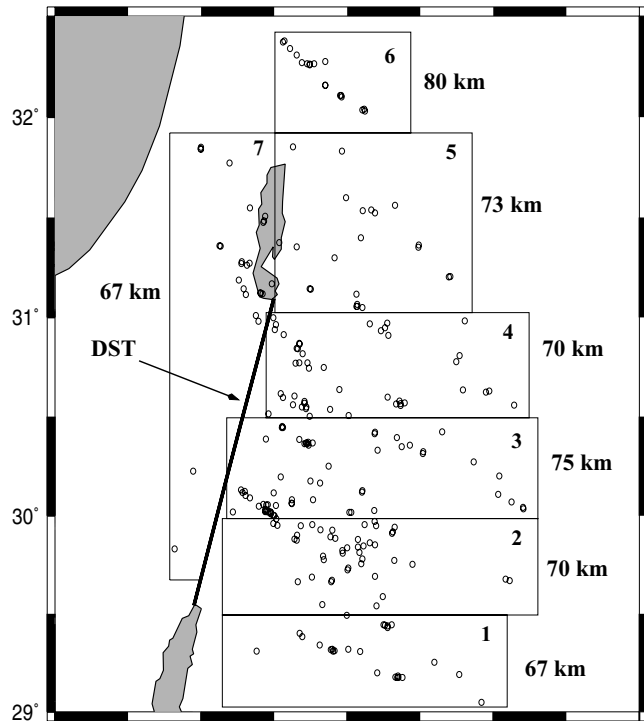

Figure 6. Distribution of *Sp* piercing points at 80 km depth. The studied area has been divided into seven non-overlapping boxes denoted by numbers. Each box contains more than 20 stacked traces. The average depth of the lithosphere is given in km beside each box.

In Fig. 6 the *Sp* piercing points at 80 km depth of all stations of the DESERT project are shown along with the boxes used for the summation. Due to the location of the usable earthquakes, nearly all piercing points are located east of the DST. Even the station EIL with more than 9 yr of data did not have a significant number of useful earthquakes from the NW quadrant. We also did not find good-quality SKS receiver functions in this backazimuth. Unfortunately, the lack of data from the west prevents us from obtaining a complete picture of the lithospheric thickness across the DST. Stations in Sinai would be needed to observe more clearly the lithosphere west of the DST.

In Fig. 7 we arranged the stacked *S* receiver functions from the DESERT temporary seismic network by the geographic locations of the piercing point boxes. Each trace in Fig. 7 shows the box number and the number of traces in the box. Zero time is the arrival time of the direct *S* arrival.

The traces are arranged with increasing order of the arrival times of the signal called LAB. This signal is clearly visible with delay times varying between 6.8 and 8 s in all boxes. Also the delay times of the Moho vary between about 4.8 and 5.3 s, corresponding to a crustal thickness about 35 km.

This is in general agreement with earlier estimates of the crustal thickness from *P* receiver functions and other seismic data in the area (e.g. DESERT Group 2004; Mohsen *et al.* 2005; Mechie *et al.* 2005; Koulakov & Sobolev 2006). The Moho and the LAB appear not to correlate with each other.

In Fig. 6 the average LAB depth in each box is also shown. The depth of the LAB varies in the investigated area along a profile of about 320 km length beginning at the Red Sea in the south to the north of the Dead Sea.

The arrival times of the LAB in seconds may be multiplied by a factor of 10 (according to the IASP91 model) to obtain the LAB
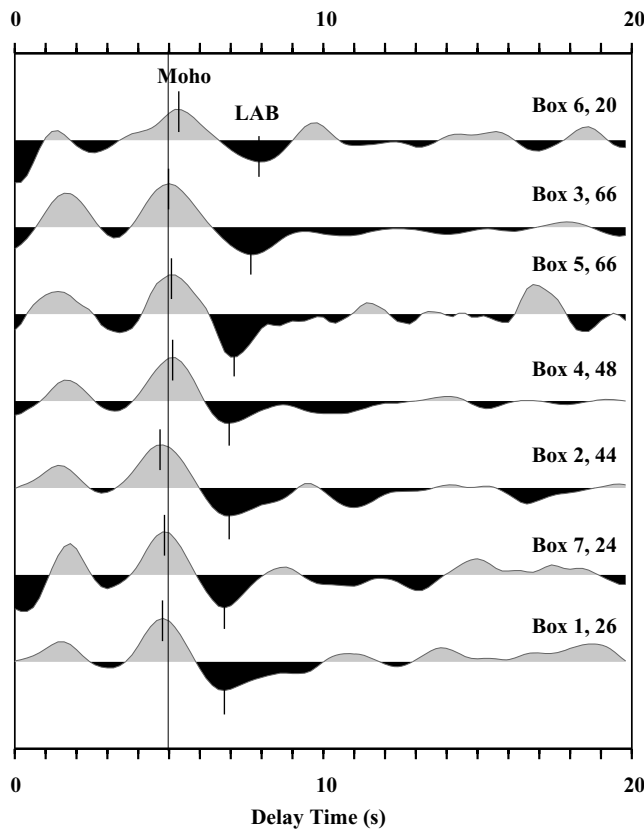
Figure 7. *S* receiver functions in the DST area. The traces are summed for each box given in Fig. 6, and the number of seismograms within each box is also given. The positive Moho phase and the negative LAB phase are visible in each box, and marked at the top. The traces are arranged with increasing order of the arrival times of the LAB. The time axis is valid for slowness of 6.4 s deg^{-1} due to moveout correction.

depth estimates in kilometres. The possible error in the depth determination is due to uncertainty in lithospheric velocity structure (estimated to be 5 per cent from tomographic results) and the selection of the times of the converted phases due to noise ($\sim$0.3 s, estimated from boot strapping) in the data. Here, we estimated the maximum error bounds due to these uncertainties as being about 5–8 km for the depth estimation. The thickness of the lithosphere changes on the eastern side of the DST from about 67 km in the south to about 80 km in the northern end of the study area. The thickness of the lithosphere in the one box west of the DST (box number 7), from few data, is about 67 km (Table 2a). In general, this would indicate that the lithosphere is slightly thinning from north to south on the eastern side of the DST (boxes 6, 5, 3, 4, 2, 1). Our determination of the thickness of the lithosphere from *S* receiver functions correlates well with the estimates from *P* receiver functions (Hofstetter and Bock 2004). The thickness of the mantle lid (LAB depth minus Moho depth) is 34 to 44 km (Table 2a). The thickness of the mantle lid for station EIL (see Fig. 1 for the location) of 53 to 62 km was reported by Hofstetter & Bock (2004), correlated with a velocity increase of the *S* waves to about 4.7 km s^{-1}.

COMPARISON WITH PERMANENT STATIONS IN THE SURROUNDING AREA

Fig. 8 shows the summed traces from the entire DESERT network including the stations JER and EIL in comparison with data from the surrounding area, Saudi Arabia (RAYN), Egypt (KEG), Cyprus (CSS) and Turkey (MALT). The number of the traces used is marked behind the station name. The Moho and the LAB are clear at most stations. The LAB at KEG seems questionable because of the noisy character of the trace. The LAB at RAYN is weak, although a large number of traces was used. This may lead to the conclusion that the asthenosphere beneath the Arabian shield is not very pronounced. The deepest Moho is observed at CSS (about 5.3 s), and the deepest LAB at RAYN.

That means the Moho and the LAB are not correlated with each other. Hofstetter & Bock (2004) have reported for station CSS the same Moho delay time using *P* receiver functions as obtained here with *S* receiver functions. The Moho delay times and the LAB advance times at the traces in Fig. 8 are, respectively: KEG: 4.65 and 7.0 s, CSS: 5.3 and 7.6 s, MALT: 4.65 and 9.0 s, RAYN: 5.0 and 16 s; that is, similar to the data at the DESERT network. The aim of this figure is to show that the Moho and the LAB are observed in the neighbourhood of the DST project as well, and to compare the results of the DESERT network with other seismic stations, using the *S* receiver function method.

DISCUSSION

The two key results of this study are (1) that regional depth of LAB is between 67 and 80 km in the DST region between Dead Sea and Red Sea and (2) that there is small, but systematic uplift of LAB towards Red Sea. Here we discuss possible implications of these results for the geodynamics of this region.

One paradox related to this region is the apparent inconsistency of the xenolith data, suggesting a hot mantle and a thin (60–80) lithosphere, and a relatively low 40–50 mW m^{-2} heat flow in the region (Ben-Avraham *et al.* 1978; Eckstein & Simmons 1979). Although recent revision of some heat flow data in Jordan (Förster *et al.* 2004, 2006) and modelling results (Petrunin & Sobolev 2006) suggest that surface heat flow in fact may have been previously underestimated (in accord with previous suggestion, Ben-Avraham, 1997), the proposed elevated values of 50–60 mW m^{-2} are still inconsistent with lithospheric thickness of 70–80 km. A possible explanation of this inconsistency is that the lithosphere of the Arabian shield has been significantly thinned recently enough (10–30 Myr ago) not to allow elevated heat flow to reach the surface (Stein *et al.* 1993; Sobolev *et al.* 2005). Alternative explanation would be that xenolith data, which are related to the local volcanic activity, represent only local conditions but not the regional thermal state of the mantle in the study area.

Our independent data indicate regionally thin lithosphere and thus clearly support the first explanation, which is also in line with the history of the regional Late Cenozoic uplift (Steinitz & Bartov 1991). Recent thermomechanical model (Sobolev *et al.* 2005) also suggests that modification of the mantle temperature is required to generate the observed asymmetrical regional uplift of the lithosphere around the DST. Based on the tectonic history of the region and modelling results it was suggested (Sobolev *et al.* 2005) that a big portion of the Arabian shield and the adjacent Mediterranean was tectonically stagnant following the Mesozoic, probably due to its location far from active mantle convection flows. This might have resulted in cooling and overthickening of the lithosphere as well as in reduced temperature of the sublithospheric mantle in the entire region. At about 20–30 Ma, due to the initiative of the Afar plume and the rifting and spreading of the Red Sea, the rejuvenation of the asthenosphere, and destabilization and thermal erosion of the

Table 2a. Differential travel time for the Moho (TTM), the LAB (TTLAB) and their difference (Dif. LAB-M) for each box in Fig. 7. The depth to the LAB and the thickness of the mantle lid were also given, based on an average Vp/Vs ratio of 1.73. The depth to the LAB was obtained by using a conversion factor of 10 (based on the IASP91 reference model). The Moho depth has been taken from Mohsen *et al.* (2005) and Hofstetter & Bock (2004).

Boxes	TTM (s)	TTLAB (s)	Dif. LAB-M (s)	D (Moho) km	D (LAB) km	Thickness of mantle lid (km)
BOX1	4.7	6.7	2.0	33.0	67.0	34.0
BOX2	4.7	7.0	2.3	34.0	70.0	36.0
BOX3	5.0	7.5	2.5	36.0	75.0	39.0
BOX4	5.1	7.0	1.9	34.0	70.0	36.0
BOX5	5.1	7.3	2.2	34.0	73.0	39.0
BOX6	5.4	8.0	2.6	36.0	80.0	44.0
BOX7	4.8	6.7	1.9	33.0	67.0	34.0

Table 2b. As Table 2(a) for average of DESERT and permanent stations.

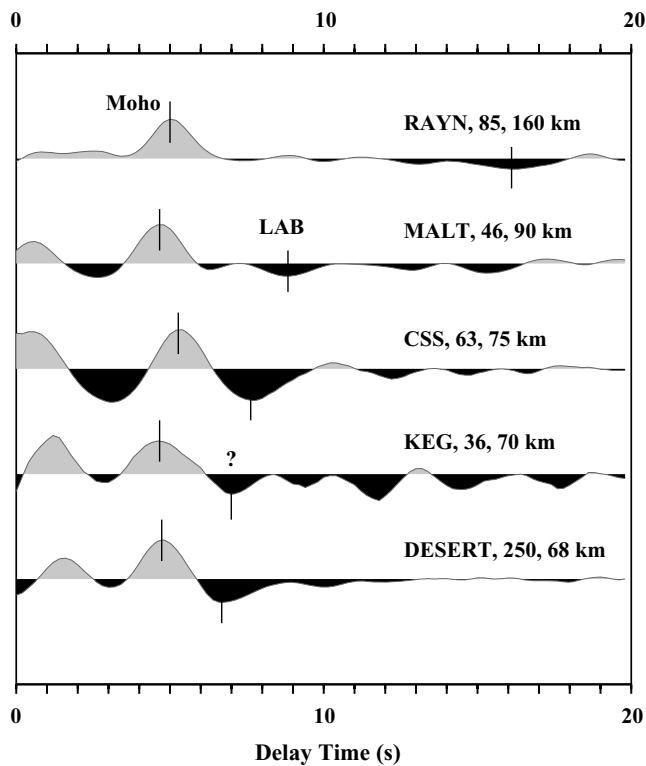| Station	TTM (s)	TTLAB (s)	Dif. LAB-M (s)	D (Moho) km	D (LAB) km	Thickness of mantle lid (km)
DESERT	4.8	6.8	2.0	35.0	68.0	33.0
KEG	4.7	7.0	2.3	36.0	70.0	34.0
CSS	5.3	7.5	2.2	32.0	75.0	43.0
MALT	4.6	9.0	4.4	40.0	90.0	50.0
RAYN	5.0	16.0	11.0	40.0	160.0	120.0

Figure 8. *S* receiver functions at the DST and the surrounding area. Each trace is the sum of each station, and DESERT is the sum of all seismic stations. The number of traces used are given together with the average depth of the LAB beside the station name. The traces are arranged with increasing order of the arrival times of the LAB. The arrival at KEG is marked by a question mark, because this station is relatively noisy.

overthickened mantle lithosphere began, resulting in the thinned lithosphere and a peak of surface uplift at 5–10 Ma. This scenario is also consistent with our second result, indicating systematic thinning of the lithosphere towards the Red Sea.

Unfortunately, due to the lack of the data we cannot confidently answer the question of how the lithosphere changes across the DST. However, from the few available data, we infer that the depth to LAB may be well the same at both sides of the DST. This result agrees with the expectation from the modelling study (Sobolev *et al.* 2005) and with the indication of no significant changes of upper mantle velocities across the DST from teleseimic tomographic study (Koulakov *et al.* 2006).

CONCLUSION

The results obtained from *S* receiver functions and those of earlier studies suggest that the DST between Red Sea and Dead Sea is characterized by a crust with an average thickness of about 35 km. Data from the temporary DESERT network show also a low-velocity zone at about 6 to 7 s, which is interpreted as the lithosphere–asthenosphere boundary (LAB).

The LAB is located at a shallow depth, of about 67 km near the Red Sea in the south and in the west of the DST. Its depth is increasing northwards to about 80 km on the eastern side of the DST. Our results confirm previous suggestions, based on xenolith data and modelling results that the lithosphere at both sides of the DST has been regionally thinned to 70–80 km recently enough not to allow elevated heat flow to reach the surface. The lithosphere at the DST is thus thinned without the concomitant of the crustal thickness. Our results also suggest an upwelling of the asthenosphere in the area, stronger in the south and weaker in the north indicating its relation with the Red Sea rift.

Members of the DESERT Group are: M. Weber,[1,5] K. Abu-Ayyash,[2] A. Abueladas,[2] A. Agnon,[3] H. Al-Amoush,[1] A. Babeyko,[1,11] Y. Bartov,[4] M. Baumann,[5] Z. Ben-Avraham,[6] G. Bock,[1] J. Bribach,[1] R. El-Kelani,[7] A. Förster,[1] H.-J. Förster,[5] U. Frieslander,[8] Z. Garfunkel,[3] S. Grunewald,[1] H.J. Götze,[9] V. Haak,[1] Ch. Haberland,[1] M. Hassouneh,[2] S. Helwig,[10] A. Hofstetter,[8] K.-H. Jäckel,[1] D. Kesten,[1] R. Kind,[1,9] N. Maercklin,[1] J. Mechie,[1] A. Mohsen,[1] F.M. Neubauer,[10] R. Oberhänsli,[5] I. Qabbani,[2] O. Ritter,[1] G. Rümpker,[1] M. Rybakov,[8] T. Ryberg,[1] F. Scherbaum,[5] J. Schmidt,[1] A. Schulze,[1] S. Sobolev,[1] M. Stiller,[1] H. Thoss,[1] U. Weckmann[1] and K. Wylegalla.[1]

[1]GeoForschungsZentrum, Potsdam, Germany
[2]Natural Resources Authority, Amman, Jordan
[3]Hebrew University, Jerusalem
[4]National Ministry of Infrastructure, Jerusalem
[5]University of Potsdam, Germany
[6]Tel Aviv University, Israel
[7]Al-Najah National University, Nablus, Palestine
[8]Geophysical Institute of Israel, Lod, Israel
[9]Free University of Berlin, Germany
[10]University of Köln, Germany
[11]Institute of Earth Physics, Moscow

REFERENCES

Abou Karaki, N., 1987. Synthese et carte seismoteconique des pays de la borrdure orientate de la Mediterranee: Sismicite du system de failles du Jourdain-MerMorte, *PhD thesis*, IPGS, Univ. Strasborg I. (In French.)

Al-Zoubi, A. & Ben-Avraham, Z., 2002. Structure of the Earth's crust in Jordan from potential field data, *Tectonophysics*, 346, 45–59.

Altherr, R., Henjes-Kunst, F. & Baumann, A., 1990. Asthenosphere versus lithosphere as possible sources for basaltic magmas erupted during formation of the Red Sea: Constrains from Sr, Pb and Nd isotops, *Earth planet. Sci. Lett.*, 96, 269–286.

Ambraseys, N., Melville, R. & Adams, R., 1994. *The Seismicity of Egypt, Arabia and the Red Sea. A historical review*. Cambridge Univ. Press. Cambridge.

Ben-Avraham, Z., 1997. Geophysical framework of the Dead Sea, in *The Dead Sea: The lake and its settings*, eds Niemi, T.M., Ben-Avraham, Z. & Gat, J., Oxford University Press, New York, pp. 22–35.

Ben-Avraham, Z., Haenel, R. & Villinger, H., 1978. Heat flow through the Dead Sea rift, *Marine Geology*, 28, 253–269.

Buttler, R. et al., 2004. The Global Seismographic Network surpasses its design goal, *EOS, Trans. Am. geophys. Un.*, 85, 23, 225–232.

Camp, V.E. & Roobol, M.J., 1989. The Arabian continental alkali basalt province, I, Evolution of Harrat Rahat, Kingdom of Saudi Arabia, *Geol. Soc. Am. Bull.*, 101, 71–95.

DESERT Group 2004. The crustal structure of the Dead Sea Transform, *Geophys. J. Int.*, 156, 655–681.

Eckstein, Y. & Simmons, G., 1979. Review of heat flow data from the eastern Mediterranean region, *Pure appl. Geophys.*, 117, 150–159.

El-Isa, Z.H., 1990. Lithospheric structure of the Jordan Dead Sea Transform from earthquake data, *Tectonophysics*, 180, 29–36.

El-Isa, Z.H., Mechie, J., Prodehl, C., Makris, J. & Khim, R., 1987a. A crustal structure study of Jordan derived from seismic refraction data, *Tectonophysics*, 138, 235–253.

El-Isa, Z.H., Mechie, J. & Prodehl, C., 1987b. Shear velocity structure of Jordan from explosion seismic data, *Geophys. J. R. astr. Soc.*, 90, 265–281.

Farra, V. & Vinnik, L., 2000. Upper mantle stratification by P and S receiver functions, *Geophys. J. Int.*, 141, 699–712.

Förster, H.-J., Förster, A., Oberhänsli, R., Stromeyer, D. & Sobolev, S.V., 2004. Lithosphere composition and thermal regime across the Dead Sea Transform in Israel and Jordan, CGU-AGU-SEG-EEGS 2004 Joint Assembly (Montreal 2004), CD-ROM, T11A–05.

Förster, A., Förster, H.-J., Masarweh, R., Masri, A., Tarawneh, K. & DESERT Group, 2006. The surface heat flow of the Arabian Shield in Jordan, *Journal of Asian Earth Sciences*, in press.

Garfunkel, Z., Zak, I. & Freund, R., 1981. Active faulting along the Dead Sea Rift, in *The Dead Sea Rift*, R. Freund & Z. Garfunkel, eds. *Tectonophysics*, 80, 1–26.

Ginzburg, A. & Ben-Avraham, Z., 1987. The deep structure of the central southern Levant continental margin, Ann, *Tectonophysics*, 1, 105–115.

Ginzburg, A., Makris, J., Fuchs, K. & Prodehl, C., 1981. The structure of the crust and upper mantle in the Dead Sea rift, in *The Dead Sea Rift*, Freund, R. & Garfunkel, Z., eds. *Tectonophysics*, 80, 109–120.

Ginzburg, A., Makris, J., Fuchs, K., Perathoner, B. & Prodehl, C., 1979b. Detailed structure of the crust and upper mantle along the Jordan-Dead Sea Rift, *J. geophys. Res.*, 84, 5605–5612.

Girdler, R.W., 1990. The Dead Sea Transform Fault System. Proc. Conf. Geol. And Tectonic process of the Dead Sea Rift zone. Standford, Calif., 7–8 Sept, *Tectonophysics*, 180, 1–13.

Götze, H.J., El-Kelani, R., Schmidt, S., Rybakov, M., Förster, H.J. & Ebbing, J., 2006. Integrated 3-D density modelling and segmentation of the Dead Sea Transform. *International J. of Earth Sciences*, doi:10.1007/s00531-006-0095-5.

Gripp, A.E. & Gorden, R.G., 1990. Current plate velocities relative to the hotspots incorporating the NUVEL-1 global plate motion model, *Geophys. Res., Lett*. 17, 1109–1112.

Hanka, W., Heinloo, A. & Jäckel, K.H., 2000. Networked Seismographs: GEOFON Real-Time Data Distribution, *ORFEUS Electronic Newsletter*, Vol. 2, No. 3.

Henjes-Kunst, F., 1989. Mantle xenoliths in western Arabia and their bearing on asthenosphere-lithosphere dynamics during formation of the Red Sea Rift. A review, Spannung und Spannungsumwandlung in der Lithosphere, Symposium on the Afro-Arabian Rift System. pp. 49–50, Karlsruhe University, Karlsruhe, Germany.

Hofstetter, A. & Bock, G., 2004. Shear-wave velocity structure of the Sinai subplate from receiver function analysis, *Geophys. J. Int.*, 158, 67–84.

Julia, J., Ammon, C.J. & Herrmann, R.B., 2003. Lithospheric structure of the Arabian Shield from the joint inversion of receiver functions and surface-wave group velocities, *Tectonophysics*, 371, 1–21.

Klinger, Y., Avouac, J.P., Abou Karaki, N., Dorbath, L., Bourles, D. & Reyss, J.L., 2000. Slip rate of the Dead Sea Transform fault in northern Araba valley (Jordan), *Geophys. J. Int.*, 142, 755–768.

Koulakov, I. & Sobolev, S.V., 2006. Moho depth and 3D P and S structure of the crust and uppermost mantle in the Eastern Mediterranean and Middle East derived from tomographic inversion of local ISC data, *Geophys. J. Int.*, 164, 218–235.

Koulakov, I., Sobolev, S.V., Weber, M., Oreshin, S., Wylegalla, K. & Hofstetter, R., 2006. Teleseismic tomography reveals no signature of the Dead Sea Transform in the upper mantle structure, *Earth. Planet. Sci. Lett.,* in press.

Kumar, P., Yuan, X., Kind, R. & Kosarev, G., 2005. The lithosphere-asthenosphere boundary in the Tien Shan-Karakoram region from S receiver functions: evidence for continental subduction, *Geophys. Res. Lett.*, 32, doi:10.1029/2004GL022291.

Kumar, P., Yuan, X., Kind, R. & James, Ni., 2006a. Imaging the colliding Indian and Asian Lithospheric plates beneath Tibet, *J. geophys. Res.*, 111, B06308, doi:10.1029/2005JB003930.

Kumar, P. *et al.*, 2006b. The Lithosphere-asthenosphere boundary of the North-West Atlantic region, *Earth planet. Sci. Lett.*, 236, 249–257.

Li, X., Kind, R., Yuan, X., Wölbern, I. & Hanka, W., 2004. Rejuvenation of the lithosphere by the Hawaiian plume, *Nature*, 427, 827–829.

Makris, J., Ben-Avraham, Z., Behle, A., Ginzburg, A., Giese, P., Steinmetz, L., Whitmarsh, R.B. & Eleftheriou, S., 1983. Seismic refraction profiles between Cyprus and Israel and their interpretation, *Geophys. J. R. astr. Soc.*, 75, 575–591.

McGuire, V.A. & Bohannon, G.R., 1989. Timing of mantle upwelling: evidence for a passive origin for the Red Sea Rift, *J. geophys. Res.*, 94, 1677–1682.

Mechie, J., Abu-Ayyash, K., Ben-Avraham, Z., El-Kelani, R., Mohsen, A., Rümpker, G., Saul, J. & Weber, M., 2005. Crustal shear velocity structure

across the Dead Sea Transform from two-dimensional modelling of DESERT project explosion seismic data, *Geophys. J. Int.*, 160, 910–924.

Mohsen, A., 2004. A receiver function study of the crust and upper mantle across the Dead sea Transform, *PhD thesis*, Freie Universität Berlin, Germany.

Mohsen, A., Hofstetter, R., Bock, G., Kind, R., Weber, M., Wylegalla, K., Rümpker, G. & DESERT Group, 2005. A receiver function study across the Dead sea Transform, *Geophys. J. Int.*, 160, 948–960.

Petrunin, A. & Sobolev, S.V., 2006. What controls thickness of sediments and lithospheric deformation at a pull-apart basin? *Geology*, 34, 389–392.

Quennell, A.M., 1958. The structural and geomorphic evolution of the Dead Sea Rift, The geological society of London *CXIV*: 1–24, London.

Sobolev, S.V., Petrunin, A., Garfunkel, Z., Babeyko, A.Yu. & DESERT Group, 2005. Thermo-mechanical model of the Dead Sea transform, *Earth planet. Sci. Lett.*, 238, 78–95.

Stein, M., Garfunkel, Z. & Jagoutz, E., 1993. Chronothermometry of peridotitic and pyroxenitic xenoliths; implications for the thermal evolution of the Arabian lithosphere, *Geochim. Cosmochim. Acta*, 57, 1325–1337.

Steinitz, G. & Bartov, Y., 1991. The Miocene-Pliocene history of the Dead Sea segment of the Rift in light of K-Ar ages of basalt, Isr, *J. Earth Sci.*, 40 199–208.

Yuan, X., Kind, R., Li, X. & Wang, R., 2006. The S receiver functions: synthetics and data example, *Geophys. J. Int.*, 165(2), 555–564, doi:10.1111/j.1365-246X.2006.02885.x.